



Bulletin of the Mineral Research and Exploration

<http://bulletin.mta.gov.tr>



Geology and formation of Nevruztepe Fe-Cu skarn mineralization (Kayseri-Turkey)

Deniz TİRİNGA^{a*}, Bülent ATEŞÇİ^b, Yılmaz ÇELİK^a, Güvenç DEMİRKIRAN^c, Cahit DÖNMEZ^a, Aytekin TÜRKEL^b and Taner ÜNLÜ^d

^aGeneral Directorate of Mineral Research and Exploration, Department of Mining and Exploration, Çankaya/Ankara, Turkey

^bGeneral Directorate of Mineral Research and Exploration, Aegean Region Directorate, Bornova/İzmir, Turkey

^cGeneral Directorate of Mineral Research and Exploration, Eastern Mediterranean Region Directorate, Çukurova/Adana, Turkey

^dAnkara University, Department of Geological Engineering, Gölbaşı/Ankara, Turkey (Emeritus)

Research Article

Keywords:

Skarn, Magnetite, Copper, Kayseri, Yeşilhisar, Yahyalı pluton.

ABSTRACT

The Nevruztepe iron-copper prospect is a skarn near Yeşilhisar (Kayseri). It has been overlooked as a potential producer of copper. The skarn was generated in Permian to Jurassic carbonate rocks by the Eocene Yahyalı granitic pluton. Lithologic units, including skarns, dip about 15 degrees southward. Skarns are both prograde (garnet and diopside) and retrograde (epidote); both exoskarn and endoskarn exist. Most of the magnetite is in a quartz-sulfide stage in retrograde skarn that is cut by veins and lenses containing quartz-pyrite-chalcopyrite. Granite and mineralized skarn are rare at the surface. From 2013 to 2015, 31 drill holes (totaling 6.178,5 m) encountered skarn to a depth of 450 m. Mineralized zones vary from 1,2 to 54,7 m thick. Fe mean grade ranges from 12% to 49%; mean copper grades vary from 10 to 4650 ppm. The deposit contains 5.096.788 tonnes of mineralized material. Microscopy on samples of drill core shows that the ore minerals are primarily magnetite, hematite, and chalcopyrite. Some magnetite is altered to hematite. Experiments show that with grinding to 100 microns the iron can be beneficiated to 66%. Waste from separation of the magnetite is 0.16 to 0.19% Cu; with flotation this was beneficiated to 19% Cu.

Received Date: 12.08.2018

Accepted Date: 10.03.2019

1. Introduction

Kayseri-Adana basin is the second most important iron province of Turkey in terms of reserve and production amounts. The Mansurlu section of the basin is riched by large-reserved hematite deposits which are oxidation products of Early Cambrian aged volcanosedimentary type siderite deposits (Tiringa et al., 2009; 2016). The best known of these deposits are Karaçat and Attepe deposits.

In the northern Kayseri-Adana basin, the Yahyalı Pluton outcrops in a narrow belt from Kovalı village

in the west, Yahyalı in the east, between Yeşilhisar and Yahyalı (Kayseri). This pluton intrudes into metamorphic units of the Yahyalı Nappe and skarn type iron and lead-zinc mineralization are formed along the contact (Hanılçı and Öztürk, 2011; Tiringa et al., 2014).

The closest mineralization to Nevruztepe Fe-Cu mineralization is Karamadazı iron deposit. Other mineralizations are called as Kovalı, Sayburnu, Kurbağapınarı and İsmailinkaya iron mineralization. All these mineralizations are actively mined as open pit, while Karamadazı iron deposit is still mining in

Citation Info: Tiringa, D., Ateşçi, B., Çelik, Y., Demirkıran, G., Dönmez, C., Türkel, A., Ünlü, T. 2020. Geology and formation of Nevruztepe Fe-Cu skarn mineralization (Kayseri-Turkey). Bulletin of the Mineral Research and Exploration. 161, 101-119. <https://doi.org/10.19111/bulletinofmre.543189>

* Corresponding author: Deniz TİRİNGA, deniz.tiringa@mta.gov.tr

galleries. In terms of type and ore paragenesis the mineralization, it has similarities with Karamadazi iron deposit.

In Karamadazi iron deposit, skarn formed as a result of contact metasomatism between quartz diorite and limestone (Oygür et al., 1978). Kuşçu et al. (2001) stated this represented typical exoskarn development and indicated that mineralization formed both endoskarn and exoskarn. The basic ore minerals in the deposit are hematite occasionally martitised and magnetite transformed to maghemite. Magnetites are accompanied by very small amounts of pyrite, chalcopyrite and pyrrhotite. The Karamadazi iron deposit has an orebody striking southeast in the form of lenses with occasional 120 m length and 20 m thickness. The deposit has proven+probable reserves calculated at 6,5 million tons with 54% Fe, 1,7% S and 11% SiO₂ (Oygür, 1986).

This study aims to determine the ore geology and formation of Nevruztepe mineralization based on mineralogic-petrographic, SEM and geochemical analysis results from drill core samples, and to attract attention to large and small iron deposits located between Yahyalı and Yeşilhisar counties, which may contain high grades of copper as well as iron. In this study, it is considered that the deposits in the region have been ignored in terms of obtaining copper from iron ore production recently, and will assess the benefit of adding this economic value for future mining activities.

1.1. Methods

Core samples are taken from ore-bearing zone to analyse trace element content and determine the grade of ore deposit. Geochemical analyses were performed in MTA General Directorate MAT Department Laboratories. Gold analyses were done with aqua regia solution and ICP-MS, silver is analysed by AAS and major oxide analyses are done with XRF. Trace element analyses were performed after triple acid solutions or aqua regia solution processes using and ICP-MS and ICP-OES.

Mineralogic-petrographic studies were performed in MTA General Directorate MAT Department Mineralogy-Petrography Laboratories with samples firstly prepared as thin and polished sections.

Thin sections were examined with Leitz polarized microscope, to determine the mineralogic, petrographic and textural properties of the rocks. Ore microscopy studies of polished sections were performed with Leica brand reflected and transmitted light microscope. SEM analysis studies were performed using FEI Quanta 400 MK2 SEM and EDAX Genesis XM4i EDS detector. For SEM analysis, polished sections are coated by carbon.

2. Geology

The study area is located in the southeast section of the Central Anatolia region, near Kovalı village located between Yeşilhisar and Yahyalı in Kayseri (Figure 1). Mainly rocks belong to the Yahyalı Nappe, outcrop in the study area and surroundings (Figure 2). Apart from these, granitic rocks of Yahyalı Pluton, the Late Cretaceous Çiftahan formation of Bozkır Assemblage, cover sediments of Palaeocene Çamardı formation and lacustrine sediments with volcanic interlayers of the middle-late Miocene Ürgüp formation are observed (Figure 3). Granitic rocks belonging to the Yahyalı Pluton in the study area are observed in a small area, which is too small to be mapped, with the ancient workings of the Sayburnu mineralization.

The Karsavuran formation is the lowest unit in the study area and surroundings. Its lowermost units are calcschist and crystallized limestone interlayered with schists and thickens upwards into limestone levels before thin to pass into schists (Ayhan and Lengeranlı, 1986). The dominant lithology in the Ayraklıtepe formation is grey-dark grey dolomite, marble and dolomitic limestones. In central sections, metacarbonate, schist and quartzite alternations are observed (Ayhan and Lengeranlı, 1986). Mostly represented by yellow, green and brown schists, the Yellibel formation comprises recrystallized limestone and calcschist interlayers containing sericite-schist, quartz-sericite schist and phyllites in some locations (Ayhan and Lengeranlı, 1986). The Başoluk formation comprises grey and yellow coloured moderate-thick-bedded quartzites (Alan et al., 2007). The dominant lithology in the Karlıgıntepe formation is grey-black coloured, fine-moderate-bedded recrystallized limestone (Ayhan and Lengeranlı, 1986). The upper sections are present in the study area represented by black, fine-moderate-bedded dolomitic levels containing micritic limestone (Tiringa et al., 2014).

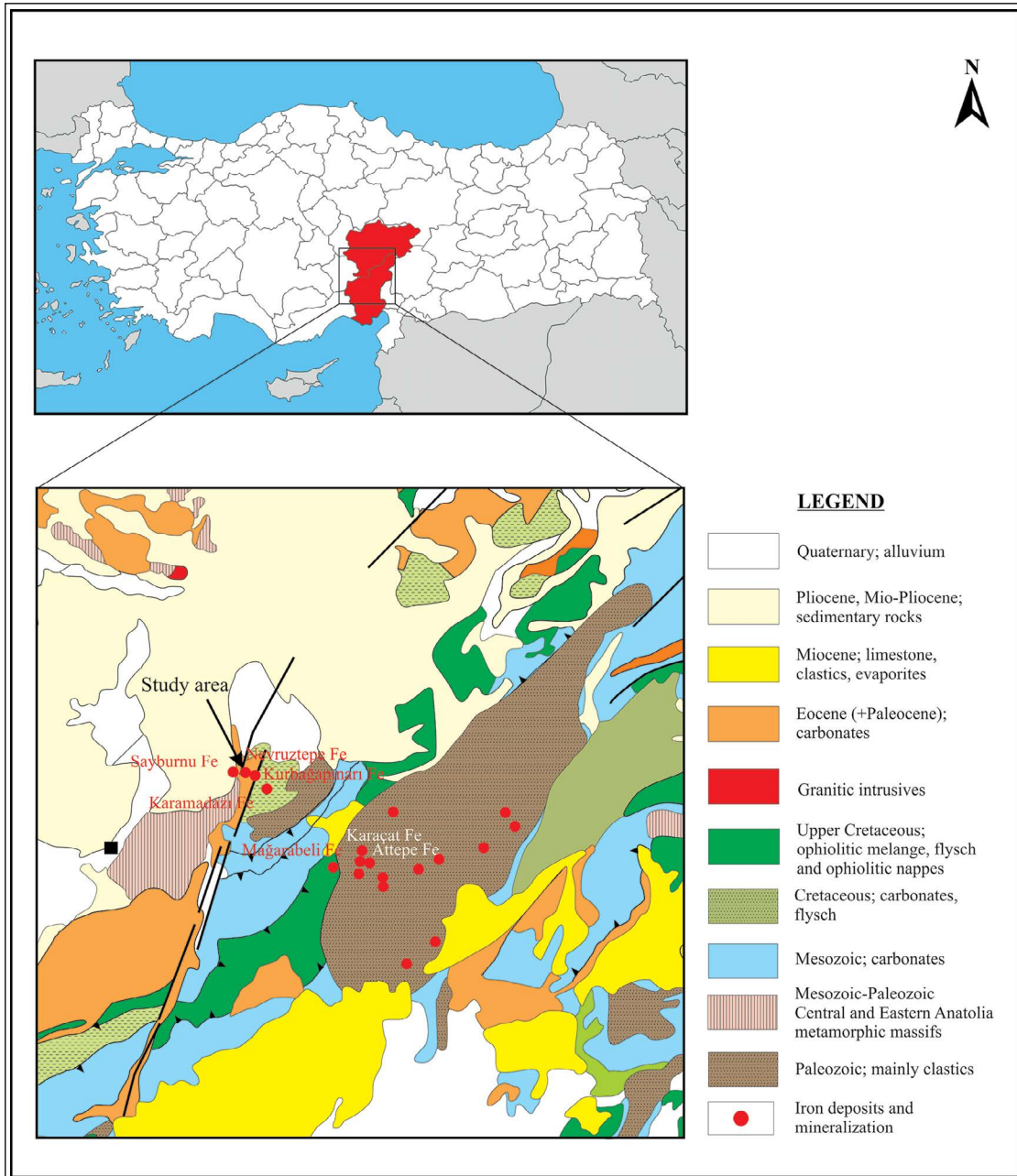


Figure 1- Location map showing regional geology of the study area and surroundings. Regional geology map taken from MTA General Directorate 1/500.000 scale geology map.

The Kocatepe formation contains recrystallized limestone, metabedstones and quartzites at lower levels (Keskin and Alan, 2013). In upper sections it comprises maroon, green, grey, yellow-grey coloured marl, mudstone and siltstone which are slightly metamorphosed (Figure 4a).

The Tavşancıdağtepe formation comprises recrystallized clayey limestone at different levels, grey-black coloured metadolomite and grey-black

coloured moderate-thick-bedded, locally very thick limestone and marble containing hematite zones, fractures filled with calcite and macro fossil shells (Keskin and Alan, 2013) (Figure 4b).

The Çiftehan formation in the Bozkır Assemblage contains serpentinites with limestone blocks, pelagic micritic mudstone, turbiditic and conglomeratic rocks, cherty limestone, radiolarite, diabase and granodiorite (Tekeli, 1980). The lowermost part of the formation

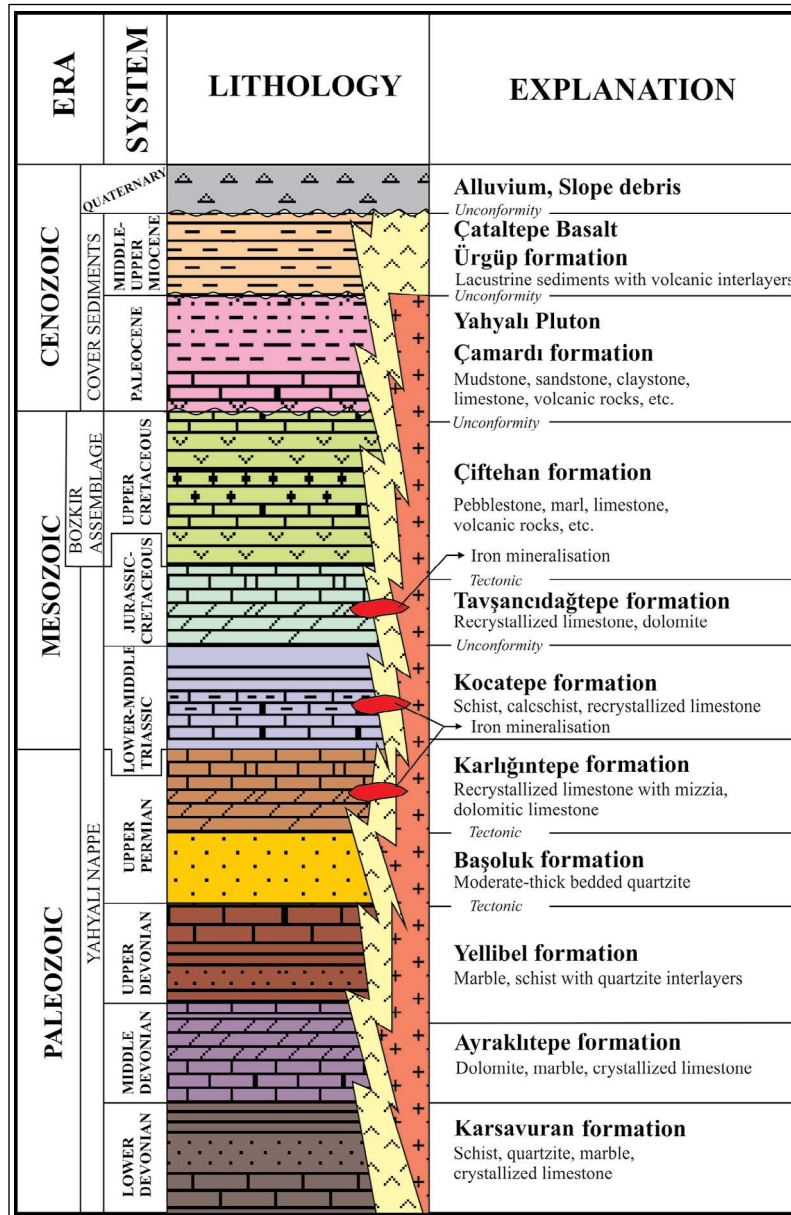


Figure 2- Generalised stratigraphic column for the study area (adapted from Keskin and Alan, 2013).

is red coloured basal pebblestone which poorly sorted pebbles up to 5 cm in size, and changes upwards to grey coloured clayey limestone and marl (Figure 4c). Marl-sandstone alternation overlies these units.

The Çamardı formation in the cover units mainly comprises marl, mudstone, siltstone, sandstone and clastic limestone. It contains rare spilitic interlayers and is cut by plutonic rocks (Keskin and Alan, 2013).

The Ürgüp formation includes red-brown coloured, poorly or without bedded pebblestone,

sandstone, mudstone, gypsum, anhydrite, limestone and ignimbrite interlayers and was deposited in continental conditions (Keskin and Alan, 2013).

The clearest outcrop of the Yahyalı Pluton is between Yularıköy and Karakuşkasası Hill. Here, it thins towards the west, and after being observed northeast of Kovalı village, east of Sayburnu, the Kovalı dam lake and in old galleries in İsmalinkaya, it is covered by younger rock units. The Yahyalı Pluton consists of calcalkaline biotite granite, quartz diorite, diorite and granodiorite. The hypabyssal

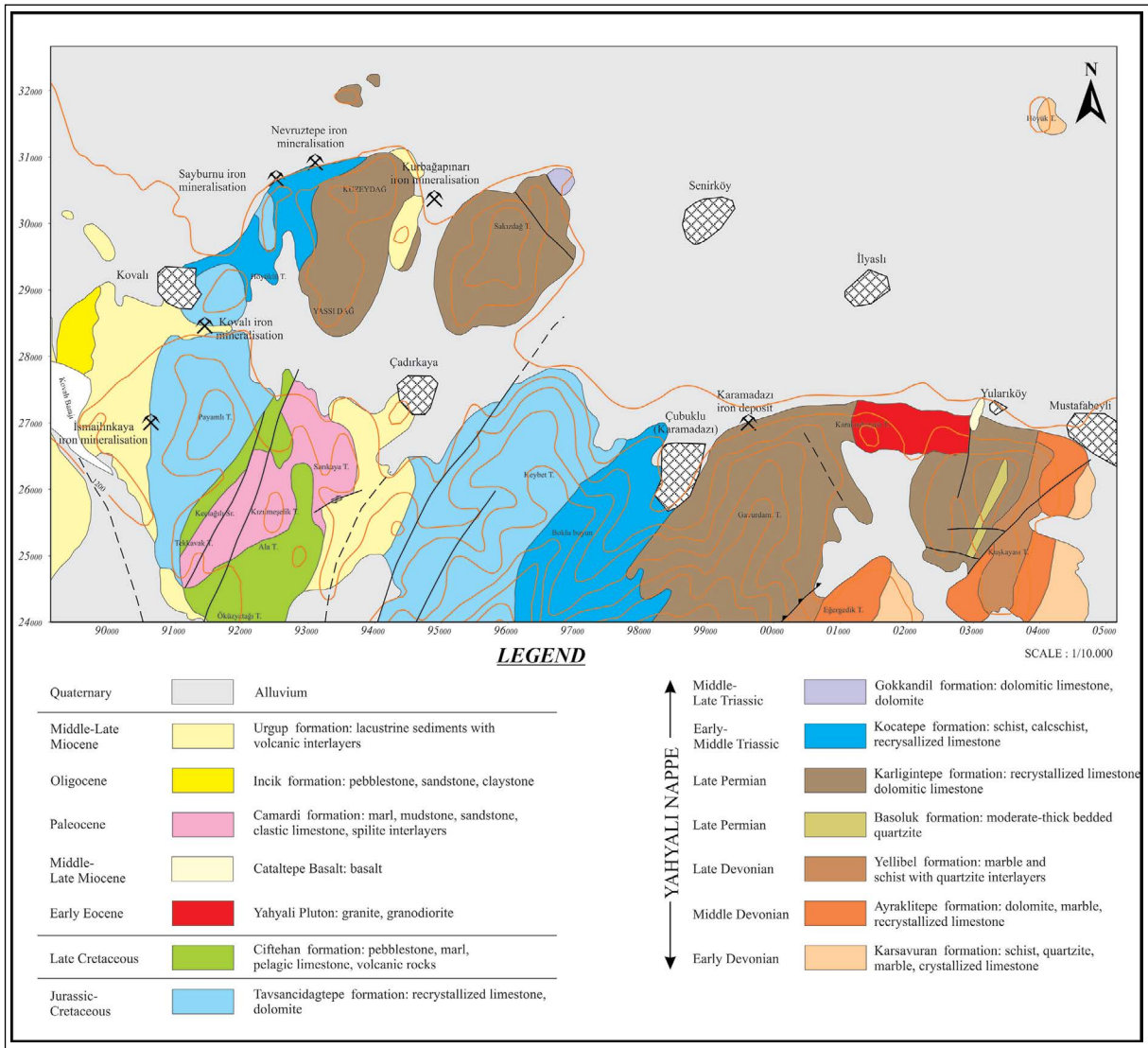


Figure 3- General geology map of the study area (taken from Keskin and Alan, 2013).



Figure 4- a) Recrystallised limestone containing quartzite-rich levels, b) Grey-coloured recrystallised limestones containing red-coloured iron zones, c) Sorted basal conglomerates belonging to the Çiftehan formation.

equivalents of these rocks of albite porphyrite, rhyolite, rhyodacite, dacite, trachydacite and andesite rocks are observed (Oygür et al., 1978). There is no reliable radiometric age data belong to the pluton.

But based on the stratigraphic relationship in the field the magmatic intrusion formed during the Eocene-Oligocene (Oygür, 1986), while Keskin and Alan (2013) proposed its age is Early Eocene.

3. Petrography

3.1. Magmatic Rocks

Mineralogic and geochemical features of the Yahyalı Pluton indicates that it is derived from typical post-collisional environment from mantle-derived mafic magma source (Boztuğ et al., 2002). During injection of the magma into the crust or during diapiric elevation through the crust, the crust melted to create coeval felsic magma association emphasising the bimodal characteristic. Another study by Kuşçu et al. (2002) compared the mean iron-copper skarn granitoids in the Yahyalı Pluton and proposed that other iron skarn granitoids contained higher Rb, Sr and Th and lower Ni, Cr, Sc and V. As a result, they stated that the granitoid should be distinguished from typical iron skarn granitoids in the world due to containing more material from the continental crust. Based on all features, the Yahyalı Pluton appears similar to the Ulukışla island arc at the end of the Late Cretaceous or beginning of the Palaeocene described by Oktay (1982) and the bimodal characteristic of Horoz (Ulukışla-Niğde) Pluton developing in post-collisional environment (Çevikbaş et al., 1995).

In this study, according to petrographic investigations of drill core samples, the magmatic rocks in the Yahyalı Pluton comprised lithologies varying from gabbroporphyry to monzonite, with basic and intermediate composition plutonic and hypabyssal rocks (Figure 5a). Additionally, many aplite and pegmatite dykes cutting the pluton and mafic enclaves up to 30-40 cm in size are observed (Figure 5b). The rocks generally have porphyritic textures, though some have holocrystalline texture. The main components are plagioclase, feldspar, biotite and quartz. Alteration is commonly observed in all rock groups. The dominant alteration in granular texture plutonic rocks like granite, granodiorite and monzonite is sericitisation, on the other hand in porphyritic rocks at the margins of the pluton argillisation and carbonation are commonly observed. Lower grade silicification and chloritisation are observed (Table 1). Considering the alteration types, it can be said that phyllic and/or argillic zones are represented. Certain rock groups determined by petrographic investigations can be listed as follows.

Monzonite-monzonite porphyry: Granular and porphyritic texture, fine-moderate grained,

plagioclase, alkali feldspar, quartz and biotite are the main components in samples. Alteration types are commonly observed as sericitisation and carbonation of plagioclase, argillisation of alkali feldspar, and chloritisation of biotite (Figures 5c and 5d).

Granite-granite porphyry, microgranite-microgranite porphyry: Rocks comprise quartz, alkali feldspar, plagioclase and biotite minerals and are fine-grained, holocrystalline and porphyritic texture. There is sericitisation, argillisation and carbonation developed in rocks, with cataclasm traces commonly observed.

Andesite: Rocks comprise plagioclase, amphibole, biotite, quartz and alkali feldspar minerals and are fine-grained with porphyritic texture. Sericitisation, argillisation, silicification, chloritisation and carbonation are observed in the rocks (Figures 5e and 5f).

Granodiorite-granodiorite porphyry: Granodiorites are the most common rock type observed in all samples. The rocks contain plagioclase, alkali feldspar, quartz, biotite and amphibole minerals and are fine-grained and granular texture. Alteration types of argillisation, sericitisation, carbonation, silicification and chloritisation are observed in the rocks (Figures 6a and 6b).

Diorite, diorite porphyry, quartz diorite, quartz diorite porphyry, microdiorite: Comprising plagioclase, biotite and amphibole minerals, the rock has fine and occasionally coarse-grain and granular texture. Alteration in the form of sericitisation, carbonation, argillisation, chloritisation, uralitisation and opacification has developed in the rock (Figures 6c and 6d).

Gabbroporphyry: One sample was defined as gabbro porphyry according to mineralogic composition, containing pyroxene, amphibole and plagioclase minerals. The rock is fine-grained with porphyritic texture, with groundmass of ophitic texture containing fine-grained plagioclase and amphibole minerals. The pyroxenes in the rock have undergone uralitisation, amphiboles have been carbonated and chloritised, while plagioclases have been argillised and sericitised (Figures 6d and 6e).

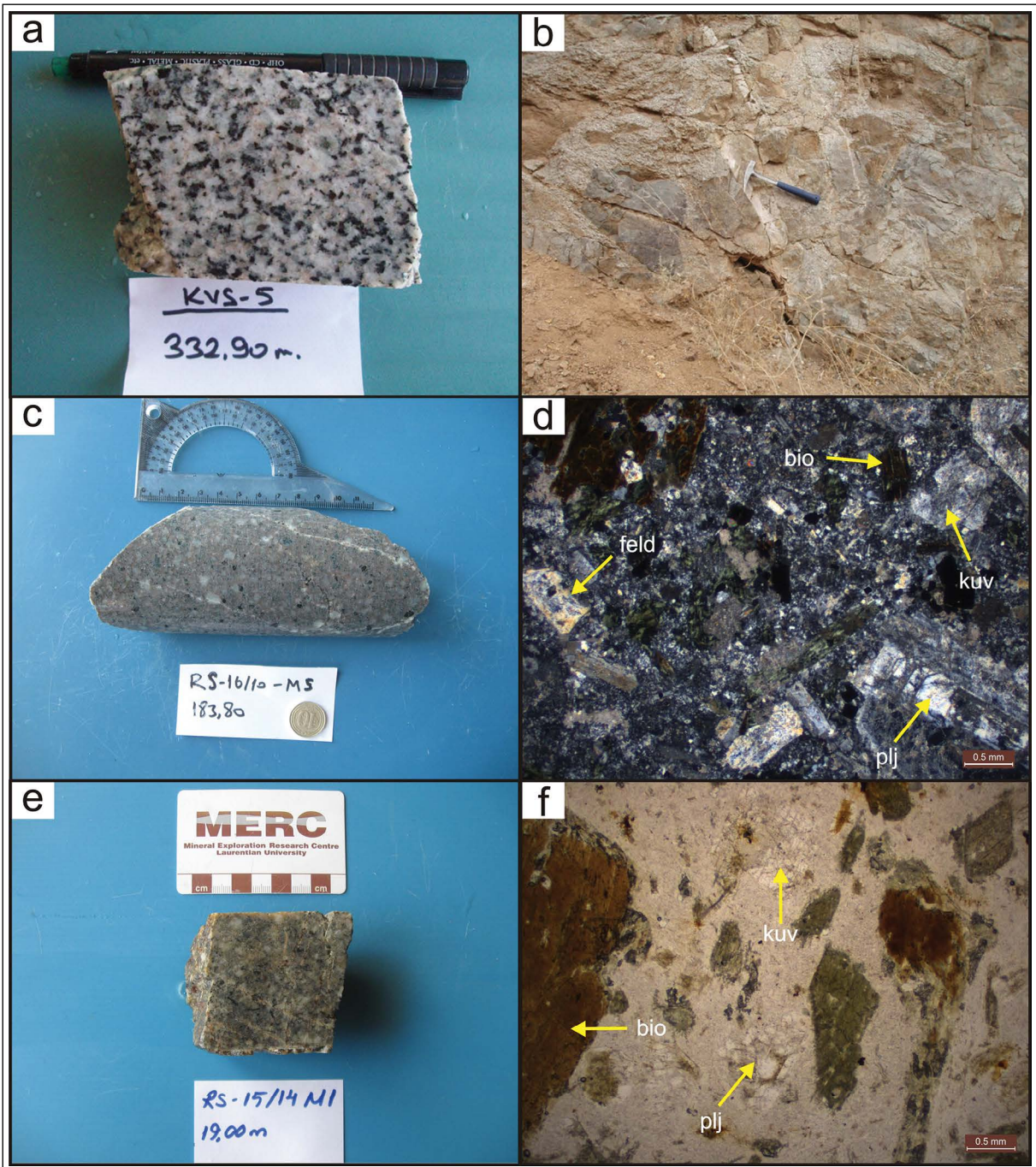


Figure 5- a) Granodiorite igneous rocks belonging to the Yahyalı Pluton, b) mafic enclaves and aplite veins commonly observed in the Yahyalı Pluton, c) monzonite core sample, d) polarising microscope image of monzonite sample (2.5 X, //), e) andesite core sample, f) polarising microscope image of andesite sample (2.5 X, //), plj: plagioclase, kuv: quartz, bio: biotite, feld: alkali feldspar.

3.2. Skarns

In the study area and surroundings, along the contact between limestone and granitoids, skarn zones are formed with very variable distribution. Due to skarn zones containing magnetite-chalcopyrite lenses with

different thicknesses, mineralization has temporal and spatial relationship with contact metamorphism and formation of skarn. Skarn lithologies do not outcrop in the locations where mineralization is observed, and so could not be mapped at preferred scale. According to petrographic and geochemical investigations within

Table 1- Summary of petrographic investigation of core samples from the Yahyalı Pluton (plj: plagioclase, amf: amphibole, px: pyroxene, q: quartz, feld: feldspar, alk. feld: alkali feldspar, horn: hornblende, lök: leucocene, kar: carbonatisation, ser: sericitisation).

| Sample ID | Grain Size | Texture | Main Components | Alteration | Rock Name |
|--------------|-------------------------------|--------------------------------|--|---|---|
| KVS-3-M9 | Fine grained | Porphyritic | plj.+amf.±apatite | clay, kar., silica | Andesite |
| KVS-5-M7 | Fine grained | Porphyritic | plj.+amf.+biotite+q± sphene | ser., clay, chlorite, kar., epidote, silica | Andesite |
| KS-14/6-M8 | Fine grained | Porphyritic | plj.+amf.+q | kar., silica, chlorite, clay | Andesite |
| KS-14/12-M1 | Fine grained | Porphyritic | plj.+amf.+px | clay, kar., chlorite | Andesite |
| KS-14/14-M6 | Fine grained | Porphyritic | plj.+biotite | chlorite | Andesite |
| RS-15/4-M5 | Fine grained | Porphyritic | px+amf.+plj.±sphene | kar., opacite | Andesite |
| RS-15/9-M4 | Fine-medium grained | Porphyritic | plj.±apatite | ser., clay, silica | Andesite |
| RS-15/10-M3 | Fine-medium grained | Porphyritic | plj.+amf.+biotite± apatite±sphene | ser., clay, opacite, silica, kar. | Andesite |
| RS-15/15-M3 | Fine-medium grained | Porphyritic | plj.+biotite+q±apatite | opacite, kar., ser., silica | Andesite |
| KVS-5-M1 | Fine grained | Porphyritic | plj.+amf.+biotite±sphene | ser., clay, chlorite, kar., epidote, uralite, silica | Andesite (include gabbro anklave) |
| RS-15/14-M6 | Medium grained | Porphyritic | plj.+biotite+amf. | ser., clay, chlorite, kar., silica, epidote | Andesite (include granular anklave) |
| KS-14/9-M4 | Fine grained | Porphyritic | q+alk feld.+plj. | kar., clay | Granite |
| RS-15/14-M2 | Fine-medium grained | Porphyritic | plj.+amf.+biotite+q | ser., clay, kar. | Andesite |
| RS-15/16-M5 | Fine-medium grained | Porphyritic | plj.+biotite+q | opacite, chlorite, kar., ser., silica | Diyoriteporphyry |
| RS-16/2-M8 | Fine-medium-coarse grained | Porphyritic | feld.+q | kar., silica | Granite |
| KVS-5-M18 | Fine-medium-coarse grained | Porphyritic | plj.+biotite+amf.± apatite±lök. | ser., clay, kar., chlorite, silica | Diyoriteporphyry |
| RS-15/16-M3 | Fine-medium grained | Porphyritic | plj.+amf.+biotite±apatite | opacite, clay | Diyoriteporphyry |
| RS-15/16-M4 | Fine-medium grained | Porphyritic | plj.+biotite+amf.±apatite | opacite, clay, silica | Diyoriteporphyry |
| KVS-6-M4 | Fine-medium-coarse grained | Porphyritic | plj.+horn.+biotite± sphene | ser., kar., epidote, chlorite, silica | Diyoriteporphyry (include monzonite ankla) |
| KVS-5-M9 | Fine grained | Granular | plj.+q+alk feld.+biotite | ser., clay, kar. | Granite |
| KS-14/8-M6 | Medium grained | Holocrystalline | q+alk feld.+plj. | kar. | Granite |
| KS-14/12-M6 | Medium grained | Holocrystalline | q+alk feld.+plj.+biotite | clay, kar., ser | Granite |
| KS-14/13-M10 | Fine grained | Holocrystalline | q+alk feld.+plj.+biotite | clay | Granite |
| KS-14/8-M9 | Fine grained | Holocrystalline | q+alk feld.+plj.+biotite | kar., clay | Granodiorite |
| KS-14/9-M7 | Medium grained | Holocrystalline | q+alk feld.+plj.+biotite | ser, clay | Granodiorite |
| KS-14/11-M3 | Fine-medium grained | Holocrystalline granular | plj+alk feld.(ortoklaz) +q+biotite+amf.±apatite | ser., kar. | Granodiorite |
| KS-14/13-M12 | Fine grained | Holocrystalline | q+alk feld.+plj.+biotite | kar., clay | Granodiorite |
| KVS-5-M13 | Fine-medium-coarse grained | Holocrystalline granular | plj.+alk feld.(ortoklaz, mikroklin)+q+biotite±sphene | ser., clay, kar., epidote | Granodioriteporphyry |
| KS-14/8-M4 | Medium grained | Hypocrystalline granular | q+alk feld.+plj.+ biotite+amf. | clay, kar. | Granodioriteporphyry |
| RS-16/4-M5 | Fine-medium grained | Holocrystalline porphyritic | plj.+amf.+q | clay, kar. | Granodioriteporphyry |
| RS-16/7-M2 | Fine-medium grained | Holocrystalline porphyritic | plj.+q+alk feld.+ biotite+amf.±titanit± zirkon±apatite | clay, kar., silica | Granodioriteporphyry |
| RS-16/10-M2 | Fine-medium grained | Holocrystalline porphyritic | plj.+q+alk feld.+amf.+ biotite±zirkon | clay, kar. | Granodioriteporphyry |
| RS-16/10-M4 | Fine-medium grained | Holocrystalline porphyritic | plj.+q+alk feld.+amf.+ biotite±zirkon±apatite | clay, kar., chlorite | Granodioriteporphyry |
| RS-15/7-M5 | Fine grained | Granular | plj+q+biotite+amf. | kar | Quartzdiorite |
| KVS-5-M14 | Fine-medium-coarse grained | Porphyritic | plj.+q+amf.+ biotite±sphene | ser., clay, kar., chlorite, silica | Quartzdiorite porphyry |
| KVS-1-M4 | Fine grained | İdiomorph granular | plj.+amf.±apatite | karb., ser., chlorite, biotite, clay | Microdiorite |
| KVS-3-M3 | Fine grained | Hypidimorph granular | plj.+alk feld.+amf. | clay, epidote, uralite, chlorite | Microdiorite |
| RS-15/15-M5 | Fine grained | Porphyritic, subophitic | amf.+biotite±apatite | kar., ser., uralit, opacite | Microdiorite |
| RS-15/6-M3 | Very fine grained | Granular | plj.+alk feld.+q+biotite | clay, ser., kar., | Micromonzodiorite |
| RS-15/4-M4 | Fine grained | Granular | plj.+alk feld.+px+amf. ±apatite±sphene | ser., clay, chlorite, epidote | Monzodiorite |
| RS-15/9-M6 | Fine-medium grained | Granular | plj.+alk feld.+q+ biotite+amf.±apatite | ser., kar., chlorite, clay | Monzonite |
| KVS-3-M12 | Fine-medium grained | Porphyritic | plj.+alk feld.+amf.+ q±sphene | ser., clay, uralit, chlorite, kar., epidote, silica | Monzonite porphyry |

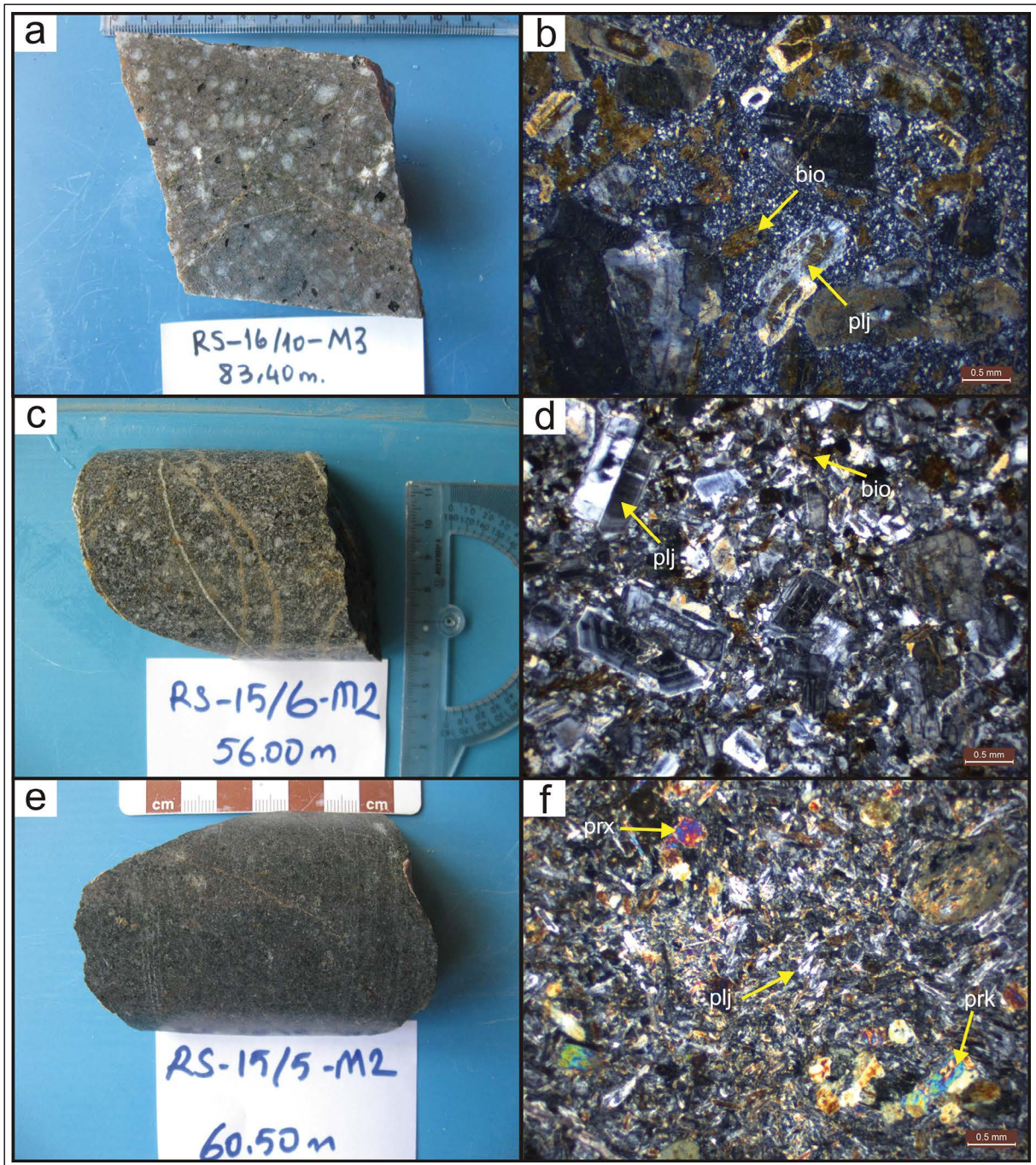


Figure 6- a) Granodiorite core sample, b) polarising microscope image of granodiorite sample (2.5 X, //), c) diorite porphyry core sample, d) polarising microscope image of diorite porphyry sample (2.5 X, //), e) gabbro porphyry core sample, f) polarising microscope image of gabbro porphyry sample (2.5 X, //), plj: plagioclase, prx: pyroxene, bio: biotite.

the scope of this study, skarns observed in Nevruztepe mineralization may be classified as calcic skarns based on wall rock composition, but the environment of skarn formation may be classified as both endoskarn and exoskarn. Garnet and epidote with rare diopside are observed as skarn minerals. The skarn minerals

indicate an oxidising environment and magnetite-rich iron and copper skarn type (Murakami, 2005). As skarn minerals are very irregular in drill core and extremely overprinted, it is not possible to describe clear mineral zonation. SEM analysis of garnet has shown they have almandine ($\text{Fe}_2+3\text{Al}_2 (\text{SiO}_4)_3$) and andradite

($\text{Ca}_3\text{Fe}_3+2(\text{SiO}_4)_3$) (Figure 7). Murakami (2005) stated that garnet with almandine type contains aluminium formed by substitution of magmatic protoliths, and hence represent endoskarn. On the other hand, andradite formed by substitution of calcium-rich wall rocks and as a result, it represents exoskarn.

Macroscopically observed garnet in drill cores is brownish coloured and coarse grained and epidote is pistachio-green coloured (Figure 8). Data obtained from microscopic investigation of garnet, epidote and diopside skarn samples is summarised below.

Diopside skarn: The rock comprises small-grained pyroxene (diopside), quartz, amphibole, carbonate,

plagioclase group minerals, chlorite, epidote and secondary components of titanite and opaque minerals with granoblastic-hornfels texture (Figures 9a and 9b).

Epidote skarn: The rock contains fine-rarely moderate grained epidote, quartz, carbonate, chlorite and secondary titanite, apatite and opaque minerals with granoblastic-hornfels texture (Figures 9c and 9d).

Garnet skarn: Rocks contain moderate-coarse grained garnet, fine-grained carbonate, amphibole and quartz with secondary components of opaque minerals with granoblastic-hornfels texture (Figures 9e and 9f).

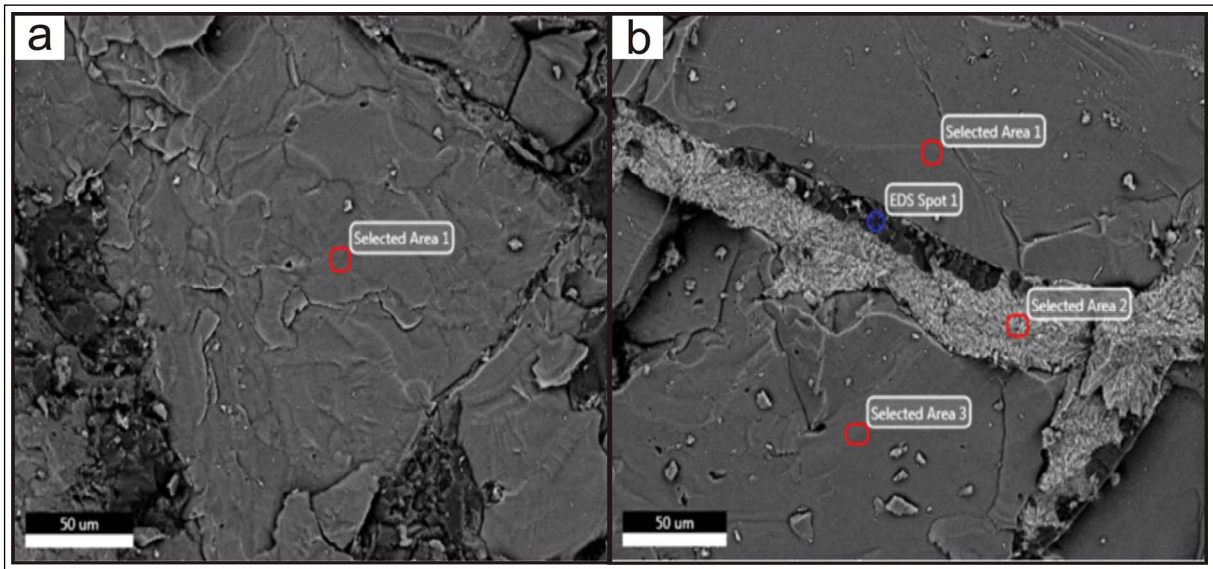


Figure 7- SEM images of core sample containing garnet, a) almandine garnet (1200 X), b) andradite garnet (1157 X).

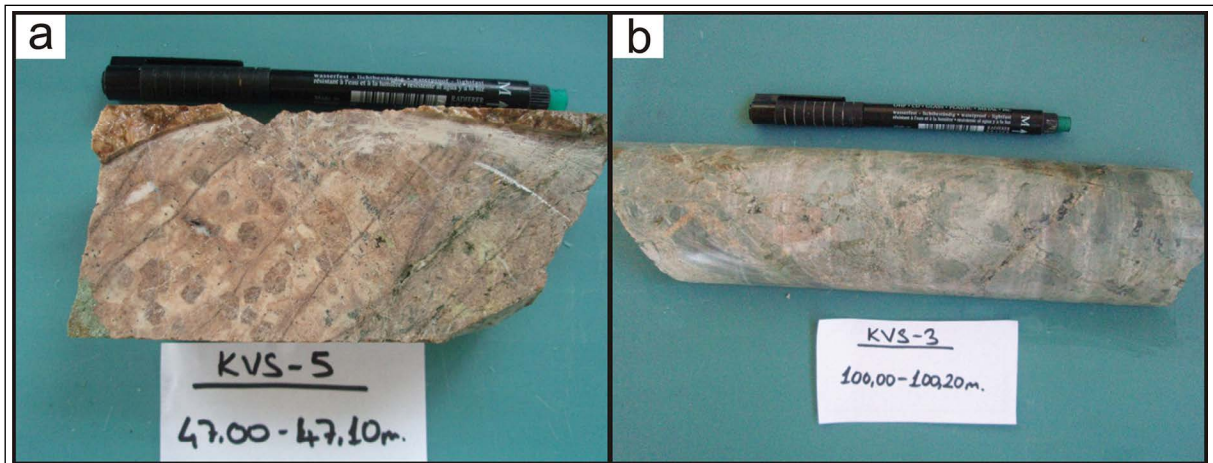


Figure 8- a) Brown-coloured garnet skarn with coarse-grain texture, b) pistachio-green epidote skarn.

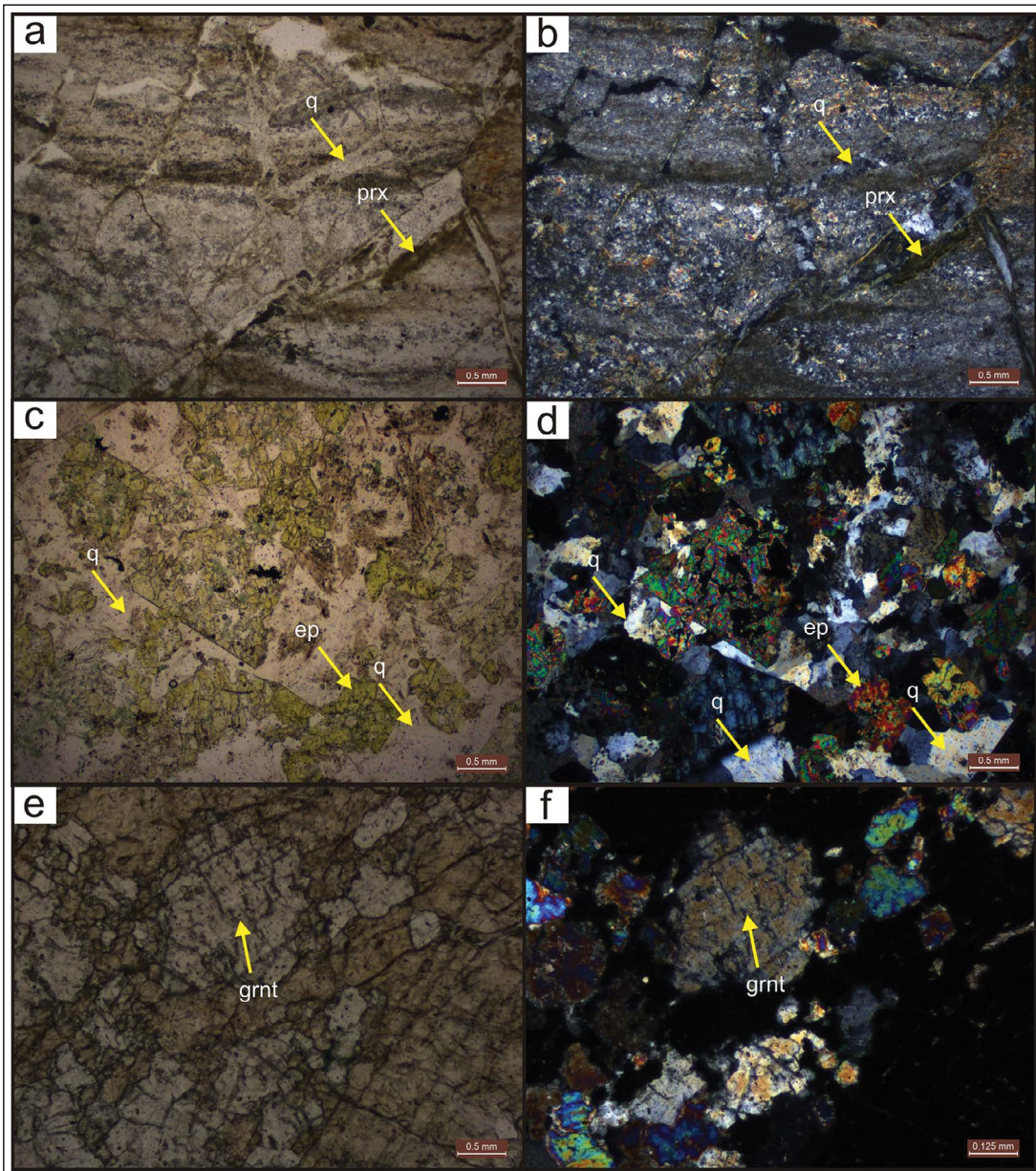


Figure 9- Pyroxene (diopside) and quartz minerals in diopside skarn rocks a) (2.5 X, /), b) (2.5 X, //); epidote and quartz minerals in epidote skarn rocks c) (2.5 X, /), d) (2.5 X, //); garnet minerals in garnet skarn rocks e) (10 X, /), f) (10 X, //), prx: pyroxene, q: quartz, grnt: garnet, ep: epidote.

4. Ore Geology

4.1. General Features of Mineralization

Yahyalı Pluton intruded into members of Yahyalı Nappes as the Early-Middle Triassic Kocatepe formation and Jurassic-Cretaceous Tavşancıdağtepe formation. The pluton outcrops close to Yahyalı county in the east and laterally continues to west, Kovalı village. Along the contact between limestone and pluton, skarn zone was developed. The most

known mineralization in this belt is Karamadazi iron deposit and it is currently operated. Nevruztepe mineralization as similar features with buried iron-copper mineralization within the same belt. In the study area, related with iron-copper mineralization, a total of 6.178,50 m of drilling was completed at 31 locations in between 2013-2016.

Nevruztepe mineralization has 750 m length along E-W trend, 500 m width and nearly 300 m thick (Figure 10). Mineralization dips toward south,

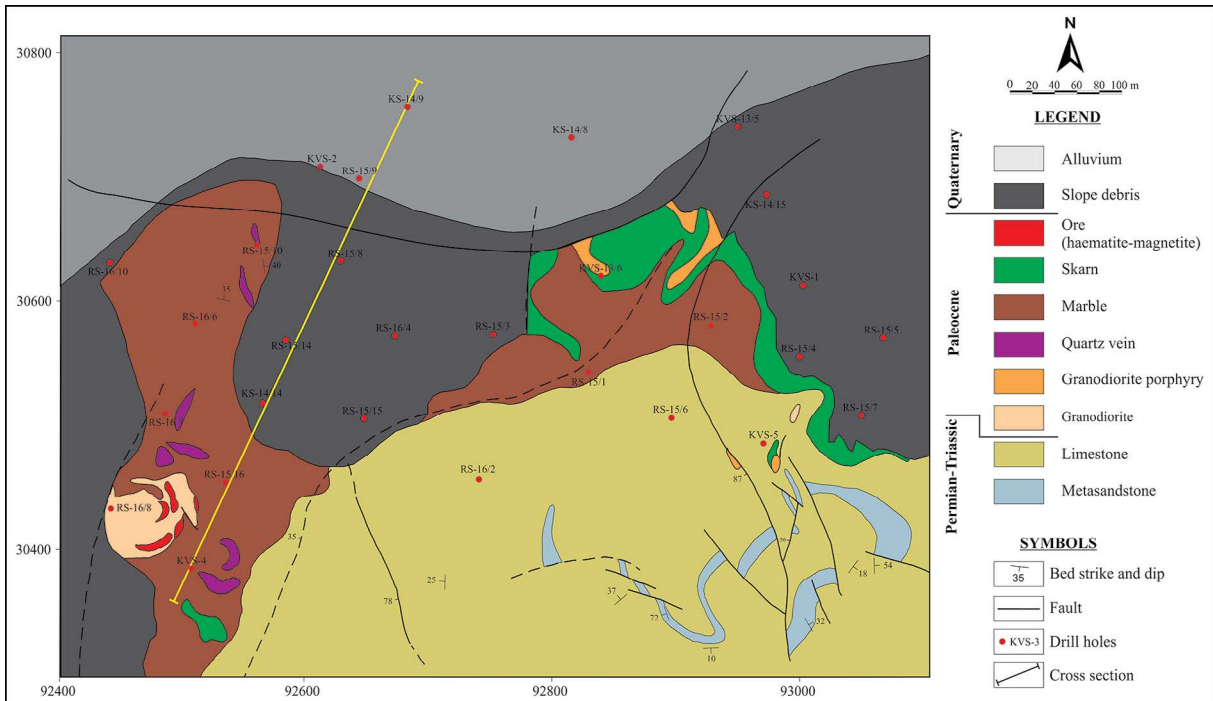


Figure 10- Detailed ore geology map of Nevruztepe Fe-Cu mineralization (Tiringa et al., 2018).

with the mineralization zone containing ore levels at different thicknesses up to 54,70 m. Mineralization is formed within skarn and magmatic intrusions. The distribution of mineralization within the magmatic intrusions is small pocket and lense shaped. Ore minerals are disseminated and/or formed in veins with different thicknesses in the skarn zone. Drill holes profiles along ore levels with different grades, and grade values correlated with mineralization level are observed on the cross-section in figure 11. Low-graded ore level extends laterally for long distances and high-graded ore levels are in lense-shaped along short distances. Copper is accompanied and enriched within iron levels.

Primary ore mineral is magnetite, which is generally anhedral and fine-grained. The main magnetite abundancy is observed along the margins, fractures and cleavages due to martitisation (Figure 12a). Hematite is observed in two forms. There is primary hematite with rod-shape as free grains, and secondary hematite is observed along fractures-cracks and cleavages due to martitisation. Along the fractures, limonitisation is also observed (Figure 12b). Ore levels contain pyrite, chalcopyrite, molybdenite, less amounts of sphalerite, bornite and malachite occasionally in limonitised zones. Pyrite is mostly

euhedral and subhedral and partly interlocking with chalcopyrite (Figure 12c). Chalcopyrite is fine-grained and interlocked with pyrite, pyrrhotite and magnetite (Figure 12d). In some samples, sphalerite exsolution is observed within chalcopyrite (Figure 12e). Molybdenite is generally submicroscopic grain, with very few rod-shaped observed within gangue minerals (Figure 12f). Sphalerite is generally fine-grained and contain chalcopyrite exsolutions. Gangue minerals are all stained with limonite, comprising diopside, feldspar (plagioclase, orthoclase), epidote, clinozoisite, quartz, biotite, chlorite, calcite and reduced oxidised garnet. Biotite is chloritised and opacified, feldspars are argillised and carbonated.

Based on field observations and petrographic studies, four paragenetic stages are defined within Nevruztepe mineralization (Figure 13). The first stage is prograde skarn stage represented by garnet and diopside minerals. This stage is characterised by formation of disseminated magnetite within garnet minerals (Figure 14a). In the second stage called as retrograde stage, magnetite as main ore mineral with epidote are dominantly observed. In this stage, less amount rod-shaped primary hematite and disseminated pyrite, chalcopyrite and pyrrhotite are observed (Figure 14b). The third stage is quartz-sulphide stage,

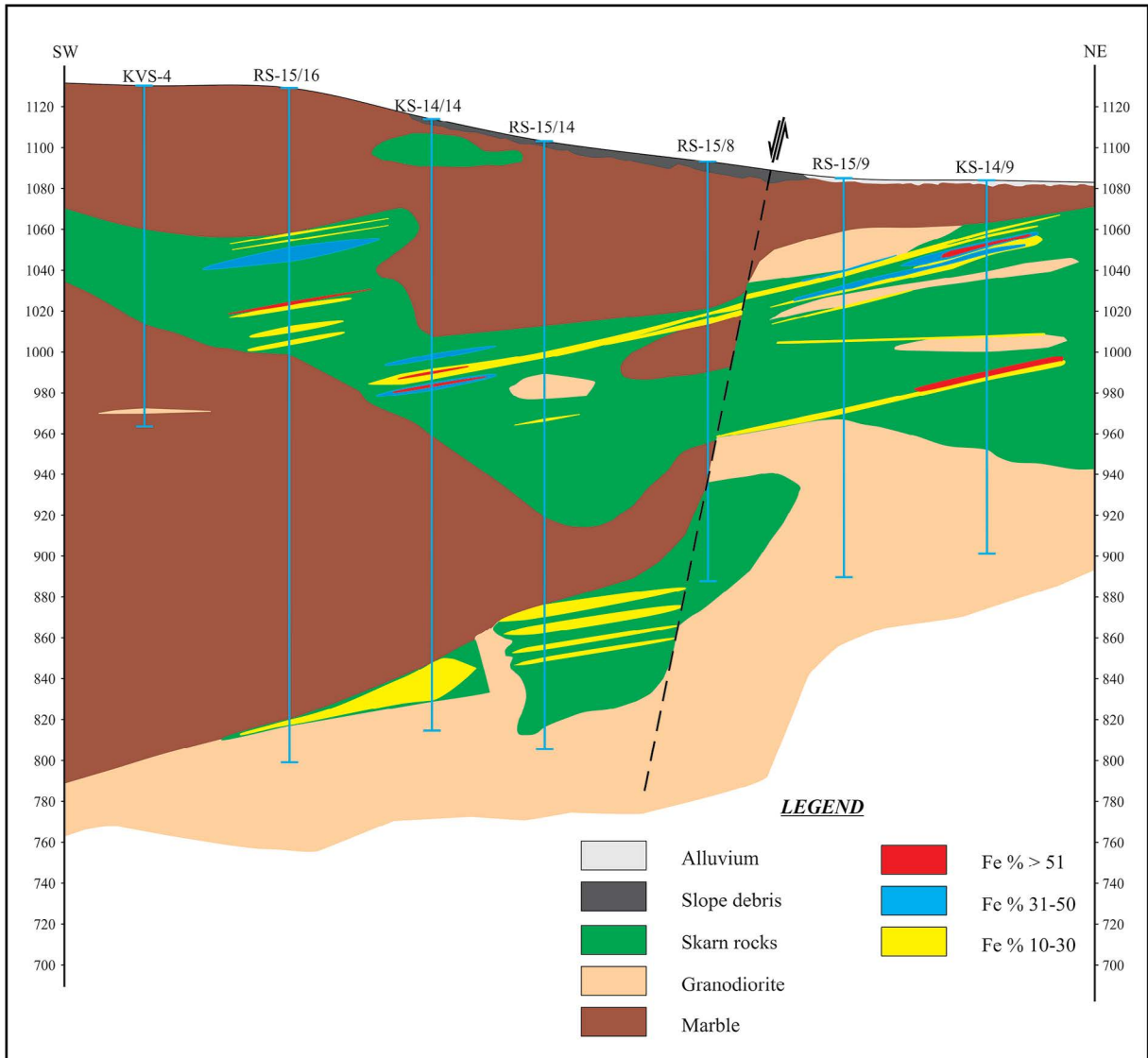


Figure 11- Geologic cross section showing drill core correlations (simplified lithologies, ore levels grouped according to grade and correlated).

and quartz-pyrite-chalcopyrite veins intensely cut by magnetites previously formed in this stage. Copper mineralization basically formed in this stage. Less amount pyrrhotite, sphalerite, molybdenite and calcite minerals are observed (Figure 14c). The fourth stage is quartz-carbonate stage. In this stage, rocks and previously formed mineralization are cut by quartz-carbonate veins. Magnetite is largely transformed to haematite due to martitisation. Limonitisation is commonly observed. Bornite, digenite, covellite and malachite transformations formed in this stage (Figure 14d).

4.2. Ore Geochemistry

Nevruztepe mineralization is low-medium grade iron-copper mineralization. Copper does not have economic importance without iron. As seen in table 2, the ore zone thicknesses are variable between 1,2 and 54,70 m, with mean Fe grade value from 12,25% up to 49,08%. Mean copper grades are also changed from 10 ppm to 4650 ppm. The elevation of SiO₂ content in iron increases the slag amount in blast furnace and energy expended by a proportional amount. As a result, the desire is that the SiO₂ content is not very high. In Nevruztepe mineralization, the mean SiO₂ is

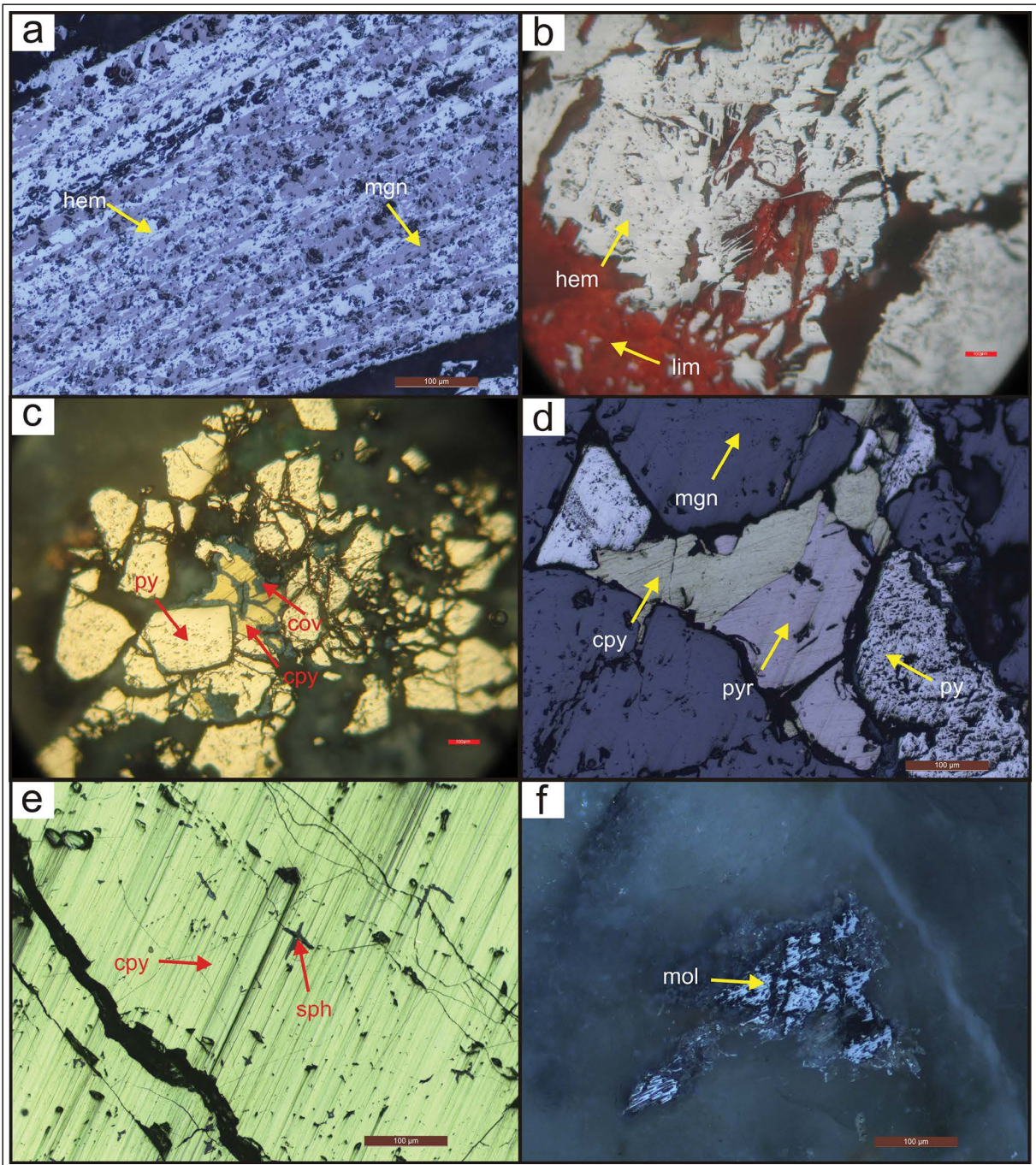


Figure 12- Microphotographs of ore microscopy studies, a) transformation of magnetite to hematite, b) hematites containing limonite in fractures, c) chalcopyrite partially transformed into covellite between pyrites, d) pyrite, chalcopyrite and pyrrhotite between magnetite, e) sphalerite separation in chalcopyrite, f) fine-grained molybdenite, mgn: magnetite, hem: hematite, lim: limonite, py: pyrite, cpy: chalcopyrite, cov: covellite, sph: sphalerite, mol: molybdenite.

high as much as 13,26% to 36,80%. The Al_2O_3 content of ore is from 0,80% to 8,78%.

Nevruztepe ore was studied by MTA with mineral processing and sample with 26,60% Fe and 0,12 ppm Cu grade ore, provided 59,66% efficiency for

66,35% Fe grade magnetite concentrate at 100-micron size. The waste from the experiment was enriched in copper content to reach 0,16-0,19% Cu grade. Flotation experiments of the waste obtained 19,48% Cu grade concentrate with 52,23% efficiency (Bayram and Bayrak, 2018).

| Stage Minerals | Prograde skarn stage | Retrograde skarn stage | Quartz-sulphide stage | Quartz-carbonate stage |
|-------------------|----------------------|------------------------|-----------------------|------------------------|
| Garnet | ————— | ————— | | |
| Diopside | ————— | | | |
| Magnetite | ————— | ————— | | |
| Epidote | | ————— | | |
| Pyrite | | ————— | ————— | |
| Chalcopyrite | | ————— | ————— | |
| Quartz | | | ————— | ————— |
| Pyrrhotite | | ————— | ————— | |
| Sphalerite | | ————— | ————— | |
| Molybdenite | | | ————— | ————— |
| Haematite | | ————— | | ————— |
| Calcite | | | ————— | ————— |
| Limonite | | | | ————— |
| Bornite | | | | ————— |
| Digenite | | | | ————— |
| Covellite | | | | ————— |
| Malachite | | | | ————— |

————— Main mineral ————— Secondary mineral

Figure 13- Mineral paragenesis and succession for Nevruztepe Fe-Cu mineralization.

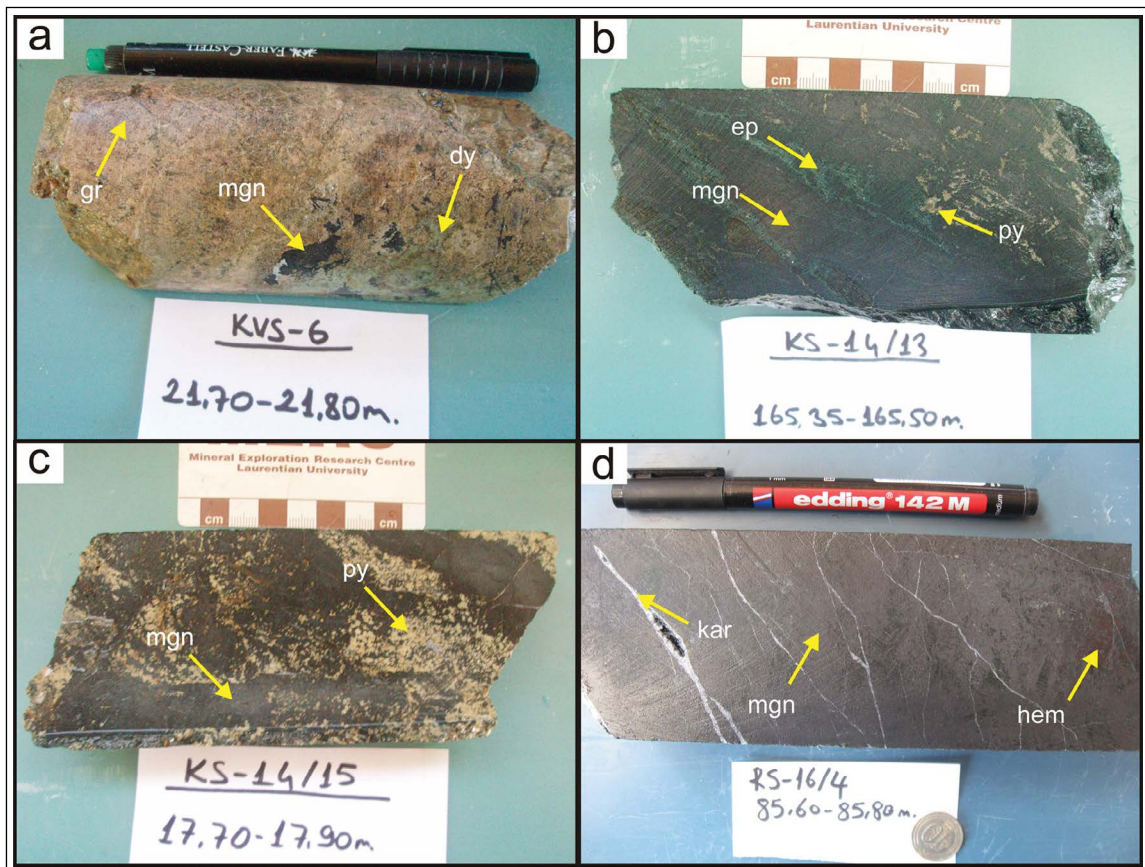


Figure 14- a) Disseminated magnetite from the prograde skarn stage, b) almost massive magnetite and secondary pyrites from the retrograde skarn stage, c) pyrite veins cutting magnetite in the quartz-sulphide stage, d) carbonate veinlets cutting magnetite and magnetite transformation hematites in the quartz-carbonate stage, gr: garnet, dy: diopside, ep: epidote, py: pyrite, kar: carbonate, mgn: magnetite, hem: hematite.

Table 2- Mean geochemical analysis results for mineralised levels cut by drill holes.

| Drill ID | Sample number (n) | Thickness of ore level (m) | Fe | SiO ₂ | Al ₂ O ₃ | S | CaO | MgO | Na ₂ O | K ₂ O | TiO ₂ | P ₂ O ₅ | MnO | LOI | Cu |
|------------------------|-------------------|----------------------------|-------|------------------|--------------------------------|------|-------|-------|-------------------|------------------|------------------|-------------------------------|------|-------|------|
| | | | % | % | % | % | % | % | % | % | % | % | % | % | % |
| KS-14/8 | 4 | 4,70 | 13,9 | 25,70 | 5,43 | 1,78 | 30,43 | 1,35 | 0,85 | 0,55 | 0,15 | 0,13 | 0,43 | 13,36 | 25 |
| KS-14/9 | 17 | 15,80 | 34,65 | 21,04 | 4,28 | 0,10 | 12,21 | 3,19 | 0,15 | 0,36 | 0,20 | 0,11 | 0,18 | 11,78 | 2717 |
| KS-14/14 | 19 | 28,90 | 27,61 | 28,54 | 2,98 | 1,59 | 19,71 | 2,28 | 0,22 | 0,26 | 0,13 | 0,10 | 0,39 | 4,44 | 1078 |
| KS-14/15 | 12 | 12,50 | 49,08 | 13,36 | 1,43 | 0,88 | 11,27 | 0,93 | 0,10 | 0,11 | 0,10 | 0,10 | 0,25 | 1,56 | 35 |
| RS-15/1 | 6 | 6,20 | 20,57 | 33,27 | 0,87 | 0,10 | 25,98 | 4,37 | 0,10 | 0,10 | 0,10 | 0,10 | 0,32 | 4,07 | 1011 |
| RS-15/2 | 27 | 54,70 | 17,39 | 33,11 | 1,39 | 0,10 | 33,04 | 2,46 | 0,10 | 0,10 | 0,12 | 0,13 | 0,43 | 4,16 | 31 |
| RS-15/3 | 3 | 3,20 | 26,92 | 22,90 | 5,73 | 0,10 | 7,23 | 13,60 | 0,17 | 0,83 | 0,20 | 0,10 | 0,10 | 10,47 | |
| RS-15/4 | 10 | 9,20 | 17,11 | 36,80 | 1,52 | 0,10 | 24,19 | 8,96 | 0,11 | 0,11 | 0,11 | 0,10 | 0,36 | 3,42 | 10 |
| RS-15/5 | 19 | 22,95 | 19,97 | 27,12 | 2,44 | 0,10 | 32,07 | 2,32 | 0,14 | 0,09 | 0,16 | 0,11 | 0,41 | 6,29 | |
| RS-15/6 | 2 | 1,90 | 12,25 | 21,95 | 0,80 | 0,10 | 35,75 | 3,75 | 0,10 | 0,10 | 0,05 | 0,10 | 0,35 | 19,60 | |
| RS-15/8 | 6 | 5,60 | 12,98 | 34,70 | 8,78 | 1,46 | 14,60 | 7,60 | 0,10 | 1,54 | 0,30 | 0,10 | 0,12 | 11,87 | 1095 |
| RS-15/9 | 10 | 12,40 | 21,38 | 30,37 | 3,79 | 2,10 | 19,37 | 5,34 | 0,14 | 0,40 | 0,15 | 0,10 | 0,33 | 8,18 | 1172 |
| RS-15/10 | 15 | 18,00 | 22,98 | 26,12 | 2,49 | 0,23 | 27,39 | 3,18 | 0,10 | 0,24 | 0,13 | 0,10 | 0,37 | 6,95 | 230 |
| RS-15/14 | 12 | 17,20 | 13,45 | 32,48 | 1,88 | 0,10 | 33,28 | 4,88 | 0,10 | 0,10 | 0,12 | 0,10 | 0,42 | 7,70 | 69 |
| RS-15/15 | 11 | 15,00 | 13,05 | 33,57 | 2,69 | 0,68 | 31,62 | 4,07 | 0,10 | 0,11 | 0,11 | 0,10 | 0,55 | 8,00 | 239 |
| RS-15/16 | 22 | 28,20 | 25,66 | 25,03 | 4,80 | 2,46 | 19,79 | 2,17 | 0,57 | 0,32 | 0,21 | 0,11 | 0,31 | 7,53 | 979 |
| RS-16/4 | 8 | 8,10 | 25,61 | 28,71 | 6,23 | 0,55 | 8,53 | 11,64 | 0,16 | 1,78 | 0,29 | 0,11 | 0,26 | 7,43 | 1060 |
| RS-16/6 | 2 | 1,20 | 29,18 | | | 8,85 | | | | | | | | | 2990 |
| RS-16/7 | 2 | 2,00 | 41,68 | | | 7,75 | | | | | | | | | 4650 |
| Overall Average | | | 24,44 | 27,92 | 3,38 | 1,53 | 22,73 | 4,82 | 0,19 | 0,41 | 0,15 | 0,10 | 0,32 | 8,04 | 1086 |

5. Discussion and Conclusion

Assessment of field observations and petrographic analyses indicates that the Nevruztepe Fe-Cu mineralization is formed by skarn processes developing Yahyalı Pluton intruded into limestones of the Yahyalı Nappe. Accordingly, Nevruztepe mineralization may be described as skarn type mineralization based on host rock, source rock, mineral paragenesis, and ore geometry parameters. As it is known, skarns deposits are formed related to regional metamorphism or contact metasomatic processes with the intrusion of magmatic intrusions into carbonate rocks. They form in intense tectonic areas where carbonate lithologies and magmatic activity is present (Einaudi et al., 1981 and Meinert et al., 2005). During skarnisation, secondary carbonates and less commonly calcium-rich silicate rocks are formed. This process is directly related with fluid movements and transporting of metals from cooling plutonic mass into surrounding rocks by the heat transfer routes, isochemical contact metamorphism and metasomatism (prograde skarn) (Pirajno, 2009). Skarn deposits are formed when pluton is hotter than 600 °C cool below 200 °C. The environmental temperature, salinity, Eh and pH

determine the type of silicate minerals formed the skarn zone (Meinert et al., 1997).

Due to temperature differences between wall rock and pluton, skarn zones develop in not only wall rock but also Yahyalı Pluton itself. In the drill core samples from Nevruztepe mineralization, thickness of skarn zone observed as more than 100 meters. Metasomatic process is highly effective on wall rock and pluton. That is why it is not so easy to distinguish endo- and exoskarn zone in the field. SEM analyses determines garnet are aluminium-rich almandine and calcium-rich andradite. Murakami (2005) proposed that aluminium-rich garnet represents the endoskarn and calcium-rich garnet indicates the exoskarn. Accordingly, Nevruztepe mineralization may be classified as both endoskarn and exoskarn based on the environment where the skarn zones are formed.

Magnetite mineralization in Nevruztepe is observed more abundantly within epidote-rich skarn zones representing the retrograde stage, and fine-grained disseminated ones are formed in the garnet- and diopside-rich skarn zones representing the prograde stage. Development of magnetite in

both the prograde and retrograde stages shows that mineralization is coeval with skarn formation. Similarly, Kuşçu et al. (2001) stated that Karamadazi iron deposit is coeval with skarnization. Oygür et al. (1978) proposed that mineralization formed as a result of metasomatism developing after skarn formation. Observations both in the field and drill cores don't indicate iron-rich lithologies within wall rocks. As a result, the only lithology that could be source for mineralization is the Yahyalı Pluton with differentiation from granodiorite to gabbro. Kuşçu et al. (2001) did not find abnormal iron enrichment or dissemination in limestone as wall rock of skarn in the Karamadazi iron deposit and proposed that the mineralization may be only related to the magmatic source and precipitated from iron solutions within late stage skarn zones. Petrographic analysis shows that retrograde stage magnetites are accompanied by a small amount of rod-shaped hematite. The quartz-carbonate stage indicates martitisation mainly along cleavages, fractures and cracks.

Nevruztepe mineralization is a low-moderate grade iron mineralization. Ore continues up to 750 m altitude with low grade, plunging to south. High-grade parts are formed as small lenses without much lateral continuity. Due to containing Cu-rich zones up to 4650 ppm in addition to iron mineralization in drill cores, the mineralization may be evaluated for copper. Copper mineralization is found with magnetite in epidote skarn from the quartz-sulphide stage, cut by pyrite-pyrrhotine and chalcopyrite veins. However, in the retrograde stage developing earlier, small amounts of disseminated copper mineralization developed within magnetites. In the final quartz-carbonate stage, chalcopyrite is changed to malachite, digenite, bornite and covellite. Technological tests were performed on Nevruztepe Fe-Cu mineralization for the first time in the region by MTA and it was revealed that after obtaining iron, copper may be extracted from waste using flotation (Bayram and Bayrak, 2018).

Total resource estimations of Nevruztepe mineralization is calculated by MTA as 5,096,788 tons at 21,05% Fe grade for iron and 1,906,267 tons of 2,219.75 ppm grade for copper (Tiringa et al., 2018). Technological tests on samples taken from drill cores obtained 66,35% Fe-grade magnetite concentration with 59,66% efficiency at 100 microns and observed that the waste was enriched in copper 0,16-0,19%

grades. Flotation experiments provided 52,23% efficiency for 19,48% Cu grade concentrate (Bayram and Bayrak, 2018).

The Karamadazi iron deposit, has almost similar geological and spatial features with Nevruztepe mineralization, is a skarn-type deposit formed by intrusion of the Yahyalı Pluton into carbonate lithologies. Skarnisation from pluton to wall rock is represented by garnet and diopside in the prograde stage and epidote in the retrograde stage. Ore is found within the epidote skarn, similar to Nevruztepe mineralization, observed as disseminated within garnet. Ore paragenesis comprises martitisation, less amounts of pyrite, chalcopyrite and pyrrhotine with great similarities to Nevruztepe mineralization. The Karamadazi iron deposit has 6.5 million tons reserve with 54% Fe, 1,7% S and 11% SiO₂ and currently mining activity is going on with underground operations (Oygür, 1986). In terms of ore geometry, Nevruztepe and Karamadazi display similarities and ore has nearly E-W striking and dipping towards south, comprising thin magnetite lenses.

Genesis, mineral paragenesis, ore minerals and succession of Nevruztepe Fe-Cu mineralization has similarities to the Handagai Fe-Cu deposit located in the north of the Great Xing'an belt in the northeast of China. The Handagai Fe-Cu deposit formed as a result of contact metasomatic processes based on geology, mineralogy and geochemical data, and is a calcic skarn formation with andradite-diopside-epidote-actinolite associations dominantly observed. Skarn formation is represented by four paragenetic stages called prograde skarn, retrograde skarn, quartz-sulphide and quartz-carbonate. Iron mineralization is observed commonly within chlorite which is formed in retrograde skarn stage. The Handagai Fe-Cu deposit is a newly-discovered deposit containing 3 million tons of iron with 30-58% grade and 18 thousand tons of copper reserve with 0,5-5,1% grade (Zhou et al., 2017).

The Astamal iron deposit within the Karadağ-Sabalan metallogenic belt in the east Azerbaijan state in northwest Iran is similar to the Nevruztepe mineralization. The Astamal iron deposit formed in a continent-continent collision environment developing after the closure of Neotethys in terms of tectonic environment linked to the intrusion of the Oligocene-aged granodioritic-quartz monzonitic Karadağ

batholith into Late Cretaceous-aged marbles. Beside the similarities of timing and lithologic features, Nevruztepe iron deposit has almost the same ore and skarn minerals, mineral paragenesis and copper production potential with Astamal iron deposit. Astamal iron deposit is the largest and richest iron deposit in northwest Iran with mean 60% grade 10 million ton iron reserve (Baghban et al., 2015).

Acknowledgements

This article is based on data obtained during studies within the scope of the Western and Central Anatolia Iron Exploration Project organised by General Directorate of MTA Department of Mining and Exploration from 2012-2016. The authors wish to thank the management of General Directorate of MTA for all aspects of their support and the Prof. Dr. Eric Cheney, Prof. Dr. Nurullah Haniçli and the other reviewers for their criticisms and recommendations about the manuscript. The authors wish also to thank Zehra Deveci Aral for her contribution to the English translation of the manuscript.

References

- Alan, İ., Şahin, Ş., Altun, İ., Bakırhan, B., Balcı, V., Böke, N., Saçlı, L., Pehlivan, Ş., Kop, A., Haniçli, N., Çelik, Ö. F. 2007. Orta Toroslar'ın Jeodinamik Evrimi, Ereğli (Konya)-Ulukışla (Niğde)-Karsanti (Adana)-Namrun (İçel) Yöresi. Maden Tetkik ve Arama Genel Müdürlüğü Rapor No: 11006, 245, Ankara (unpublished).
- Ayhan, A., Lengeranlı, Y. 1986. Yahyalı-Demirkazık (Aladağlar Yöresi) Arasının Tektonostratigrafik Özellikleri, Jeoloji Mühendisliği Dergisi 27, 31-45.
- Baghban, S., Hosseinzadeh, M. R., Moayyed, M., Mokhtari, M. A. A., Gregory, D. 2015. Geology, mineral chemistry and formation conditions of calc-silicate minerals of Astamal Fe-LREE distal skarn deposit, Eastern Azarbaijan Province, NW Iran. Ore Geology Reviews 68, 79-96.
- Bayram, A. İ., Bayrak, M. Y. 2018. Kayseri-Yeşilhisar Demir Cevherinin Zenginleştirme Çalışması. Maden Tetkik ve Arama Genel Müdürlüğü MAT Dairesi Arşivi, Ankara (unpublished).
- Boztuğ, D., Çevikbaş, A., Demirkol, C., Tatar, S., Akyıldız, M., Otlu, N. 2002. Karamadazı Plütonunun (Yahyalı-Kayseri) Mineralojik-Petrografik ve Jeokimyasal İncelemesi. Türkiye Jeoloji Bülteni 45, 1, 41-58.
- Çevikbaş, A., Boztuğ, D., Demirkol, C., Yılmaz, S., Akyıldız, M., Açlan, M., Demir, Ö., Taş, R. 1995. Horoz Plütonunun (Ulukışla-Niğde) Oluşumunda Dengelenmiş Hibrid Sistemin Mineralojik ve Jeokimyasal Kanıtları, TJK Bülteni 10, 62-77.
- Einaudi, M. T., Meinert, L. D., Newberry, R. J. 1981. Skarn Deposits, Economic Geology, 75th Anniversary 317-391.
- Haniçli, N., Öztürk, H. 2011. Geochemical/Isotopic Evolution of Pb-Zn Deposits in the Central and Eastern Taurides, Turkey. International Geology Review 53, 13, 1478-1507.
- Keskin, H., Alan, İ. 2013. Yahyalı (Kayseri)-Dündarlı (Niğde) Arasında Kalan Alanın Jeolojisi (Doğu Toroslar'ın Jeodinamik Evrimi ve Metalojenezi Projesi), Maden Tetkik ve Arama Genel Müdürlüğü Rapor No: 11612, 50, Ankara (unpublished).
- Kuşçu, İ., Gençlioğlu Kuşçu, G., Göncüoğlu, M. C. 2001. Karamadazı Demir Yatağında Skarn Zonlanması ve Mineralojisi. Türkiye Jeoloji Bülteni 44/3, 1-14.
- Kuşçu, İ., Gençlioğlu Kuşçu, G., Saraç, C., Meinert, L. D. 2002. Jeokimyasal Karakterizasyon Çalışmalarında Faktör Analizi Yönteminin Kullanımı: Çelebi Granitoyidi ve Karamadazı Graniti. Türkiye Jeoloji Bülteni 45/1, 125-140.
- Meinert, L. D., Hefton, K. K., Mayes, D., Tasiran, I. 1997. Geology, zonation, and fluid evolution of the Big Gossan Cu-Au skarn deposit, Ertsberg District, Irian Jaya, Econ. Geol. 92, 509-534.
- Meinert, L. D., Dipple, G. M., Nicolescu, S. 2005. World skarn deposits, Econ. Geol. 100th Ann. 299-336.
- Murakami, H. 2005. How to Study Skarn Type Deposits. A short time expert seminar in MTA, Ankara.
- Oktay, F. Y. 1982. Ulukışla ve Çevresinin Stratigrafisi ve Jeolojik Evrimi. Türkiye Jeoloji Bülteni, 25/1, 15-24.
- Oygür, V., Yurt, F., Yurt, M. Z. 1978. Kayseri-Yahyalı-Karamadazı ve Kovalı Yöresi Demir Madenleri Jeolojisi, Maden Tetkik ve Arama Genel Müdürlüğü Rapor No. 6609, Ankara (unpublished).
- Oygür, V. 1986. Karamadazı (Yahyalı-Kayseri) Kontak Metazomatik Manyetit Yatağının Jeolojisi ve Oluşumu, Jeol. Müh. Dergisi 27, 1-9.
- Pirajno, F. 2009. Hydrothermal Processes and Mineral Systems, Australia, Springer 1250.
- Tekeli, O. 1980. Toroslar'da Aladağlar'ın Yapısal Evrimi, Türkiye Jeoloji Bülteni 23/1, 11-14.
- Tiringa, D., Ünlü, T., Sayılı, S. 2009. Kayseri-Yahyalı-Karaköy, Karaçat Demir Yatağının Maden

- Jeolojisi. Jeoloji Mühendisliği Dergisi, Jeoloji Mühendisleri Odası Yayınları 33/1, 1-43.
- Tiringa, D., Ateşçi, B., Türkel, A., Tufan, E., Akın, U., Yıldırım, G. 2014. AR: 201201149 ve AR: 201300002 (Kayseri-Yeşilhisar) ile AR: 201201150 (Kayseri-Yahyalı) Nolu Ruhsat Sahaları Maden Jeolojisi Ara Raporu. Maden Tetkik ve Arama Genel Müdürlüğü Rapor No: 11753, Ankara (unpublished).
- Tiringa, D., Ünlü, T., Gürsu, S. 2016. Erken Kambriyen Yaşlı Karaçat Demir Yatağı (Mansurlu Havzası, Adana) ve Doğusunda Yüzeyleyen Demir Yataklarının Kökenine Bir Yaklaşım. Maden Tetkik ve Arama Dergisi 152, 121-141.
- Tiringa, D., Ateşçi, B., Çelik, Y., Türkel, A., Demirkıran, G., Niğdeli, S. F., Yurtseven, D., Yakıcı İçli, M., Aksoy, T. 2018. Kayseri-Yeşilhisar-Kovalı Yöresindeki AR: 201201149 (ER: 3286890) no'lu IV. Grup Ruhsat Sahasına Ait Demir ve Bakır Madenleri Buluculuk Talebine Esas Maden Jeolojisi ve Kaynak Tahmin Raporu. Maden Tetkik ve Arama Genel Müdürlüğü Rapor No: 13742, Ankara (unpublished).
- Zhou, Z., Mao, J., Che, H., Ouyang, H., Ma, X. 2017. Metallogeny of the Handagai Skarn Fe-Cu Deposit, Northern Great Xing'an Range, NE China: Constraints on Fluid Inclusions and Skarn Genesis. Ore Geology Reviews 80, 623-644.

